atmosphere

MDPI

Article

Climate Variability of Atmospheric Rivers and Droughts over the West Coast of the United States from 2006 to 2019

Paul R. Zechiel and Sen Chiao *

Department of Meteorology and Climate Science, San Jose State University, San Jose, CA 95192, USA; paul.zechiel@sjsu.edu

* Correspondence: sen.chiao@sjsu.edu; Tel.: +1-408-924-5204

Abstract: Water resources are crucial to the livelihood and sustainability of the general public across the western United States. This study covers the timespan of both the third driest drought in Californian history between 2012 and 2015 as well as the extreme atmospheric river year in 2016–2017. The evaluation of vertical moisture profiles using Constellation Observing System for Meteorology, Ionosphere, and Climate (COSMIC) Radio Occultation (RO) data, National Centers for Environmental Prediction (NCEP)/National Center for Atmospheric Research (NCAR) Reanalysis of 500 hPa geopotential heights, 1000–500 hPa thickness, Optimum Interpolation (OI) Sea Surface Temperature (SST), NOAA/NDBC buoy data, and NASA, MEaSUREs, Gridded Sea Surface Height Anomalies (SSHA) were performed. The daily COSMIC time evolution from 2006 through 2015 showed a flat to slightly upward trend of both temperature and water vapor profiles through the entirety of the western US drought. Subsequently, a significant increase of temperatures and water vapor were recorded in early 2016 before the extreme Atmospheric River (AR) season of 2016–2017. The quantitative analyses suggest that warmer SST and higher SSHA lead to an increase of heat fluxes from the ocean into the troposphere, which forces thickness changes and thus the position of troughs in the geopotential height field changes afterwards, consequently pushing the trough eastward over the Pacific Northwest and potentially leading to an active AR year in the western US. It appears that regional COSMIC RO moisture profiles, seasonal SST, and SLH anomalies may serve as a precursor for seasonal or sub-seasonal precipitation outlook along the western US.

Keywords: atmospheric rivers; drought; COSMIC; satellite; climatology; reanalysis; geopotential heights; thickness; sea level heights; sea surface temperatures; buoys

Citation: Zechiel, P.R.; Chiao, S. Climate Variability of Atmospheric Rivers and Droughts over the West Coast of the United States from 2006 to 2019. *Atmosphere* **2021**, *12*, 201. https://doi.org/10.3390/atmos12020201

Academic Editor: Jonathan Jones
Received: 13 December 2020
Accepted: 26 January 2021
Published: 3 February 2021

1. Introduction

Atmospheric Rivers (ARs) are responsible for over 90% of the poleward water vapor transport, while only covering about 10% of the global longitudinal area (Neiman et al. 2008b; Rutz et al. 2014) [1,2]. Roughly 60–74% and 33–40% of droughts in the Pacific Northwest and California, respectively, have ended due to the arrival of AR storms (Dettinger 2013) [3]. Atmospheric River events are an essential source of moisture and precipitation that are observed along the west coast and are a key factor in the prevalence of droughts and floods. Nevertheless, water resources are critical issues that California is facing today and will continue to face amidst the threat of global climate change. In California, three-fourths of the population and their water demands are primarily in the central and southern parts of the state, while two-thirds of the precipitation and runoff occurs in the northern one-third of the state (Dettinger 2011) [4]. Furthermore, global environmental changes have potentially increased flooding threats along the western United States after multi-year droughts (Dettinger 2011) [4]. Considering the ability to end droughts and the geographic disparity of California's resources, understanding the strength and climatology of ARs and their impact on the west coast is essential for water management, reservoir operations, and the mitigation of flood risks.

It is currently a matter of prodigious public and scientific interest how ARs and droughts have activity changed over the western United States and will further change in a warming climate. Although theory and modeling consistently suggest a climatological change of extreme events in a warming climate, confidence in detecting the change of ARs or droughts in historical data remains low, and this can only be addressed by better understanding the associated mechanisms (Dettinger 2011) [4]. Existing numerical models may not be sufficient to correctly forecast such situations in advance. Investigating the response of the precipitation of ARs and droughts to climate change is complicated. It is also not well understood because the data in the northeastern Pacific are generally limited, making it difficult to determine the mechanisms in relation to droughts or extreme weather events over the west coast. For instance, California experienced the third hottest and driest season on record in 2016, but it was less extreme compared to 2014 and 2015. However, an AR event associated with extreme rain caused inland floods in early 2017. It would be useful to evaluate the past and the possible future using useful multiple data sources (e.g., satellites, models, and in-situ measurements) regarding extreme precipitation events and droughts in California and along the west coast of the United States.

Using the Constellation Observing System for Meteorology, Ionosphere, and Climate (COSMIC) data, Anthes et al. [5] summarized that COSMIC would contribute to improved global analysis and forecasts of climate variability and climate change. Anthes et al., (2001) [5] explains that, especially in remote oceanic regions, COSMIC water vapor profiles would enable scientists to monitor the response of the global atmosphere to regional events such as atmospheric rivers. Wang (2017) [6] analyzed the COSMIC data from 2007 to 2016, which demonstrated that a significant warming has occurred during that time period, and most pronounced warming areas had occurred over the polar region. The pronounced warming over the polar region is exacerbating sea ice loss and melting glaciers. Trenberth and Guillemot (1996) [7] concluded that satellite data has allowed scientists to validate the direct relationships between Sea Surface Temperature (SST) variations and synoptic-scale circulation patterns. Chen and Leung (2020) [8] explained that warmer SSTs along the Western United States did increase the total amount of landfalling ARs. Furthermore, Chen and Leung (2020) and Dai et al. (1998) [8,9] articulated that global climate models have shown that, as global SST rises, the total amount of evaporation into the atmosphere increases, consequently increasing the likelihood of extreme events. They concluded that warmer SSTs directly caused by increased evaporation will provide an increase of moisture upstream of AR development (Chen and Leung 2020) [8]. On the other hand, Koustavas et al. (2006), Stott et al. (2004), and Barron et al. (2003) [10–12] suggested that cooler SSTs in the eastern Pacific directly forced by positive radiative forcing events and global warming does increase the likelihood of droughts in California. In terms of western US precipitation, El Niño amplifies the subtropical jet and storm track in southern California and Mexico. On the other hand, La Niña occurs when, in the central and eastern Pacific Ocean, SSTs cool and the easterlies amplify (National Oceanic and Atmospheric Administration (NOAA) US Department of Commerce 2020) [13]. La Niña leads to a variable Pacific jet stream, forcing the storm track poleward. In addition to SSTs and (El Niño-Southern Oscillation (ENSO), Penduff et al. (2019) [14] studied the trends of coastal sea levels. They found that, over 17–20% of the global ocean coastal area, random sea-level trends may complicate their atmospherically forced counterpart (Penduff et al. 2019) [14]. Nevertheless, from a climatological aspect, the relationship between atmospheric vapor, sea surface height, atmospheric rivers, and droughts may still need to be explored further.

The overarching goal of this paper is to perform a comprehensive study about the attributes and factors that lead to droughts and ARs. Using Constellation Observing System for Meteorology, Ionosphere, and Climate (COSMIC), National Centers for Environmental Prediction (NCEP)/National Center for Atmospheric Research (NCAR) Reanalysis, NASA Making Earth System Data Records for Use in Research Environments (MEaSUREs) Sea Surface Temperature, and (National Data Buoy Center) NDBC Buoy data will allow this study to evaluate extreme precipitation events and droughts during the wet season of

California from 2006 to 2019 in order to discern if the strength of ARs are increasing compared to previous years and also investigate the variability of droughts. Comparisons will then be made to a 13-year record of COSMIC data along the eastern Pacific coast. The methods used to provide these comparisons will be described in Section 2, followed by data and results in Section 3, and our concluding results and recommendations for future work can be seen in Section 4.

2. Data and Analysis Methods

2.1. COSMIC Vertical Profiles

University Corporation for Atmospheric Research (UCAR's) Constellation Observing System for Meteorology, Ionosphere, and Climate (FORMOSAT-3/COSMIC) mission was launched in 2006 as a joint research project by Taiwan and the United States [15]. COSMIC consists of a constellation of six small polar orbiting satellites that are distributed equally around the Earth, providing users with extensive data coverage over data-sparse locations including oceans and inhabited land. Furthermore, Ho et al. (2019a) [16] states that, through 2016, COSMIC has offered users approximately 1000 soundings a day and one sounding for each 5° × 5° latitudinal box. Radio occultation (RO) employs active satellites that use Global Navigation Satellite System Radio Occultation (GNSS-RO) measurements to accurately vertically profile the Earth's atmosphere (Ho et al. 2019a) [16].

Each satellite consists of three instruments, which include the following: a GPS radio occultation receiver that receives radio waves from a GPS satellite, an ionospheric photometer that measures the strength of electromagnetic waves throughout the Earth's ionosphere, and a tri-band beacon (e.g., Very High Frequency, Ultra High Frequency, and L-Band) which is a device that provides the satellite with a bearing by locating the radio waves Constellation Observing System for Meteorology Ionosphere, and Climate (COSMIC) 2020; UCAR Community Programs 2020) [17,18]. COSMIC satellites intercept radio signals from other GNSS satellites in orbit and measures their bending and signal delay (UCAR Community Programs 2020) [18]. After refracting the radio waves, COSMIC then relays the data down to the COSMIC Data Analysis and Archive Center (CDAAC) with vertical profiles of the following parameters: temperature, pressure, water vapor, bending angles, and refractivity (UCAR Community Programs 2020) [18].

The target area that was analyzed in this study, as shown in Figure 1, consists of the eastern Pacific Ocean and the western mid-latitudes from the Washington/Canadian border through California (30° N to 50° N and 140° W to 120° W). To conduct this study, a historical COSMIC time series of daily moisture profile's (WetPrf) were processed from June 2006 through March 2019. Each daily profile included a mean vertical profile of the following variables: pressure (P) [Pa], temperature (T) [°C], vapor pressure (VP) [Pa], and calculated mixing ratio (r) [g/kg] (Equation (1)) values from the lowest level to 5 km above ground level.

$$r = \left(0.622 \times \left(\frac{VP}{P - VP}\right)\right) \times 1000, \quad (1)$$

The lowest level to 5 km profiles were evaluated in this study (denoted as 0–5 km) to depict how the moisture and temperature profiles changed between the surface and the mid-atmosphere. In order to improve interpretation in the study, each COSMIC plot included the daily value (marked as red dots) and running means of weekly, monthly, seasonal, and annual trends. COSMIC data after March 2019 was excluded in this study because only one of the six satellites remained online, consequently leading to a plethora of missing data and an abundance of inaccuracies in the dataset. COSMIC data was made available by the Data Analysis and Archive Center Constellation Observing System for Meteorology Ionosphere and Climate (University Corporation for Atmospheric Research) [19].

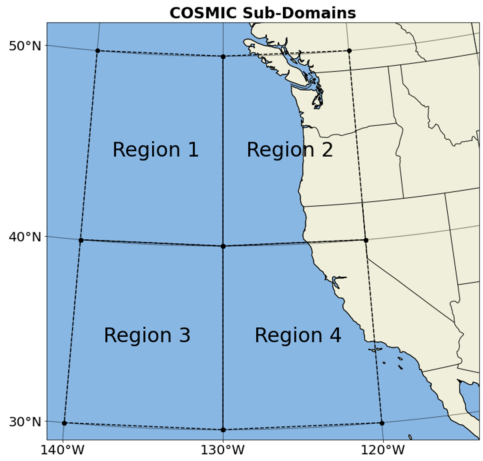

Figure 1. The target area of the Constellation Observing System for Meteorology Ionosphere, and (COSMIC) vertical profiles collected in this study. Four sub-domains were created for further analysis of regional meteorological variables, as seen in Sections 3.2.1–3.2.3.

2.2. Regional Climate Characteristics

Global reanalysis from the NCEP/NCAR Reanalysis Project, Kalnay et al. (1996) [20], were used in this study to plot and analyze 500 hPa geopotential heights and 1000–500 hPa thickness. Each variable studied will portray autumn (SON) and winter (DJF) seasonal anomalies for the purpose of comparing seasonal and sub-seasonal variations in the dataset. In order to develop a 30-year anomaly dataset, the researched seasonal anomalies were calculated by taking the mean of each seasonal group (i.e., SON and DJF) from January 1989 through March 2019. Quantitative tables were developed to average out each of the variables in their domains to provide future statistical analysis. Additionally, the original target area was then divided into four sub-regions consisting of a 10° × 10° latitudinal box to display the spatial distributions of each analyzed variable (See Figure 1). The first sub-domain was designed to pertain to the Pacific Northwest and cover part of the northeastern Pacific from 40° N to 50° N and 140° W to 130° W. Next, sub-domain 2 encompasses western/central Washington, Oregon, and the northern tip of California. (40° N to 50° N and 130° W to 120° W). Sub-domain 3 includes the northeastern Pacific between the bounds of 30° N to 40° N and 140° W to 130° W. Finally, the fourth and final sub-domain encompasses northern California to the United States/Mexico border (30° N to 40° N and 130° W to 120° W). The focus of the regional scale analysis was designed to identify climatological patterns and explain how they directly affect the location of landfalling western United States AR events.

NASA JPL Making Earth System Data Records for Use in Research Environments (MEaSUREs 2015) [21] were employed to evaluate the sea surface height variations over the target area. MEaSUREs provides a high resolution global (0.17° × 0.17°) analysis dataset with a 5-day temporal resolution of sea surface height and sea surface height anomalies. The NASA JPL MEaSUREs sea level heights are constructed by the kriging method from two simultaneous sets of altimetric satellites (MEaSUREs 2015) [21]. The first set of simultaneous satellites include the TOPEX/Poseidon, Jason-1, Jason-2, and Jason-3, while the second set of satellites include the ERS-1, ERS-2 Envisat, AltiKa, Cryosat-2, and Sentinel 3A. Furthermore, in terms of accuracy of sea level heights, MEaSUREs (2015) [21] shows a reliable solution of approximately −1 to 0 cm error term from 1993 to 1999 and a positive 0 to 1 cm error through 2015.

From an in-situ observations perspective, NOAA National Data Buoy Center (NDBC) offers quality measurements across broad marine environments. NOAA NDBC (2020) [22] states that, since the early 1980's, buoys have been deployed to spatially cover the western Atlantic to the northeastern Pacific. Furthermore, NOAA NDBC (2020) [22] has installed 50 Coastal-Marine Automated Network (C-MAN) buoys and over 100 meteorological buoys

that provide information on barometric pressure, wind direction, wind speed, wind gust, and air temperature.

The NOAA 1/4° daily Optimum Interpolation (OI) Sea Surface Temperature (SST) V2 data (Zlotnicki 2019) [23] was used to evaluate the annual and seasonal differential of sea surface temperatures throughout the domain. OISST data is constructed by combining observations from different platforms (satellites, ships, buoys, and Argo floats) on a regular global grid. A spatially complete SST map is produced by interpolating to fill in gaps. The methodology includes bias adjustment of satellite and ship observations (referenced to buoys) to compensate for platform differences and sensor biases (Zlotnicki 2019) [23].

The Climate Prediction Center (2020) [24] ENSO amplitude archive was used to monitor El Niño and La Niña conditions. ENSO amplitudes are found by taking a 3-month running mean of SST anomalies between 5° N and 5° S to 120° W and 170° W (Climate Prediction Center 2020) [24]. In addition to the amplitudes, El Niño/La Niña is broken down into categories to portray the severity of the event. Therefore, a weak ENSO amplitude has 0.5 to 0.9 SST anomaly, moderate 1 to 1.4, strong 1.5 to 1.9, and very strong when SST is greater than 2 (Null 2020) [25].

The National Weather Service (NWS) (Advanced Hydrologic Prediction Center 2020) [26] rain gauges were used to evaluate the daily precipitation accumulation around the San Francisco Bay Area (e.g., region 4 in Figure 1). These rain gauges are well maintained and accurate; however, inaccuracies can occur due to the following: freezing precipitation, windy conditions, and obstructions (Advanced Hydrologic Prediction Center 2020) [26].

3. Results

3.1. COSMIC Moisture and Temperature Observations and Annual Features

Time evolution of COSMIC moisture profiles were conducted in association with the seasonal and sub-seasonal variability of mixing ratio and temperature characteristics of the target region. Additionally, heat maps of moisture were added to portray any seasonal trends or patterns that were observed during the study.

The first COSMIC variable investigated in this study was mixing ratio. When visualizing the monthly averages, the seasonality of the mixing ratio is clearly observed, with the highest peak found in the summer months. The summer month peaks are due to an increase of solar radiation to the surface, consequently forcing an increase of latent heat release into the atmosphere. As shown in Figure 2, the historical time series depicts a slight decreasing trend ~−0.19 g/kg (~−0.047 g/kg/year) of vertical profile mixing ratio from July 2006 through early 2013. This slight decrease of mixing ratio between 2011 through 2014 is analogous to the extreme western United States drought, which greatly reduced the moisture field upstream of the resilient ridge in the Pacific Northwest. Between late 2015 and 2016, the mixing ratio trend line showed the steepest climb of ~0.32 g/kg (~0.162 g/kg/year). Afterwards, starting in October 2016 through early 2017, the annual mixing ratio trend line peaked and remained constant at ~2.8 g/kg. In 2018, the trend line appeared to decrease again by ~0.2 g/kg and flatlined around ~2.6 g/kg. The observed decrease of mixing ratio in 2018 was directly attributable to a persistent ridge hovering along the entire west coast, forcing storm tracks northward.

The magnitude of mixing ratio was processed via heatmaps in order to further analyze the trends and patterns of mixing ratios in the target region. The analysis includes both Figure 3a normalization of mixing ratios and Figure 3b mixing ratio anomalies. Both heatmaps were limited to October through March in order to focus on how the mixing ratio changed during the climatological west coast rain season. As shown in Figure 3a, the heat maps predominantly showed lower than average mixing ratios in the winter months (DJF) for years 2006 through 2014, with the lowest values during the drought. A shift in DJF mixing ratios, starting in 2015–2016, was observed and peaked in the extreme AR rain season of 2016–2017. The anomalies showed near average mixing ratio values from 2007–2011 before the beginning of the drought (Figure 3b), the highest positive anomalies were found in 2016–2017, and a slight decrease of positive anomalies was seen through

2019. The key finding observed in the heatmaps (red dashed line) was a possible wave-like oscillation. Future investigation will be needed to determine if the observed wave maintains the same wave period and if the wave can be directly influenced or linked to any climatological oscillations. This future research could provide a possible summary of when the western United States may see the next drought and/or extreme AR rain season.

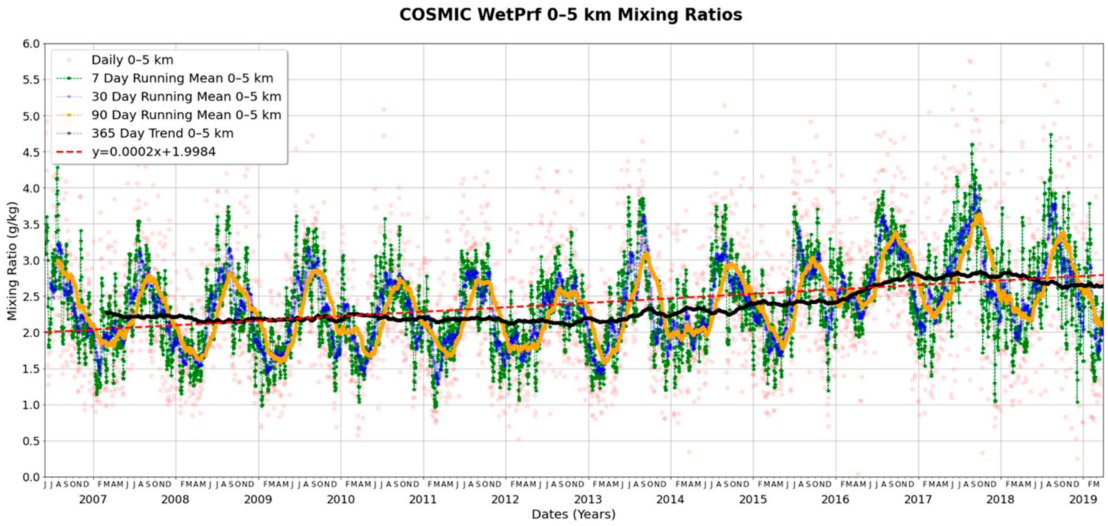

Figure 2. COSMIC Mixing Ratio from 0–5 km in the target domain.

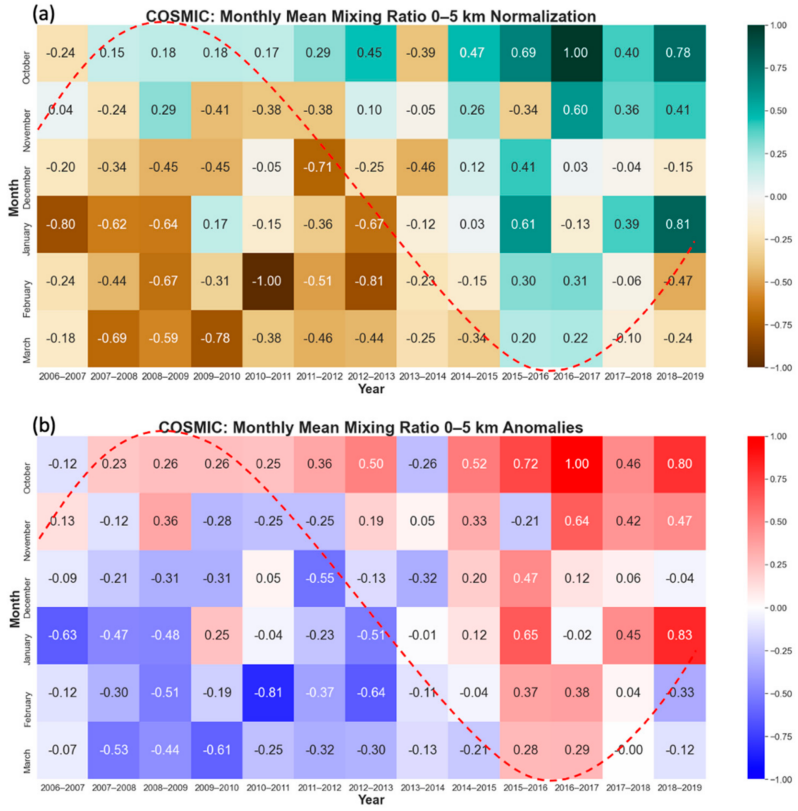

Figure 3. COSMIC mixing ratio heatmaps: (**a**) 0–5 km normalization and (**b**) 0–5 km anomalies.

The second COSMIC variable that was investigated was the 0–5 km (i.e., lowest level to 5 km above ground level (AGL)) temperatures (Figure 4). Similar to patterns seen in the moisture field, temperatures in the domain decreased by ~−2.10 °C (~−0.52 °C/year)

from June 2006 through late 2013. In order to compare the average 5 km profile with in-situ surface observations, eight sets of buoy data from NDBC were analyzed (Figure 5). Buoy data showed the warmest surface temperatures in 2014 through 2015, however, the COSMIC temperature profile observed the warmest temperatures in 2016. According to Phillips and Leslie (2017) [27], 2016 global average temperatures witnessed the warmest year in the last 137 years of recorded data. Furthermore, they suggested that a strong El Niño in early 2016 directly increased the global temperature by approximately 0.5 °C from the 1981–2010 mean (Phillips and Leslie 2017) [27]. The enhanced global warming in 2016 helped induce an increase of latent heat release and consequently affected western United States precipitation in the 2016–2017 rain season. After the above average rain season in 2016–2017, both COSMIC and buoy temperatures showed a decrease by approximately 1 °C. Potentially, the cooler temperatures observed by COSMIC in late 2017 forced a decrease of latent heat into the atmosphere. Therefore, with less moisture and a persistent 500 hPa ridge along the west coast, California saw a tremendous reduction of moisture leading to a below-average rain season in 2017–2018. Temperatures within the target area rebounded in early 2018, consequently evaporating more water into the atmosphere, leading to another above average rain season in 2018–2019.

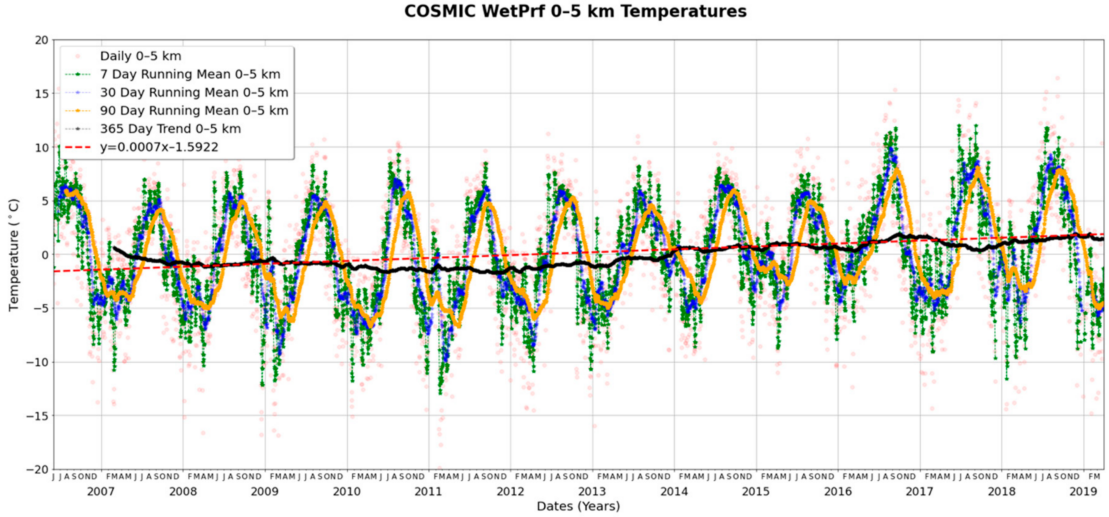

Figure 4. COSMIC temperature evolutions (i.e., 0–5 km) in the target area.

3.2. Regional Analysis

This section explores the reanalysis data for a few important large scale meteorological factors. Analysis will include seasonal anomaly maps from 2006 through 2019 of 500 hPa geopotential heights with 1000–500 hPa thickness, sea level heights (SLH), and sea surface temperatures (SSTs). Additionally, for each variable analyzed, a quantitative table was constructed to organize the data and to highlight potential trends and patterns.

3.2.1. 500 hPa Geopotential Heights and 1000–500 hPa Thickness

The results of 500 hPa geopotential heights with 1000–500 hPa thickness [20] overlaid are shown in Figure 6a,b. During the autumn and winter seasons between 2006 and 2011, the western United States observed oscillating weak positive and negative height and thickness anomalies. The offsetting pattern of weak anomalies displayed a more neutral and undisturbed environment during this time span. In 2012, the western United States observed the beginning of its 3-year long drought. During the drought, a predominant moderate to strong positive height and thickness anomaly was observed, and it was enhanced by an onshore push of an upper-level ridge. Similar results were seen by Swain (2015) [28], who explained that the persistence of a ridge in the Pacific Northwest stayed from 2012 through 2015 and directly contributed to the drought. Furthermore, Wang

et al. (2014) [29] suggested that the downstream trough that brought cold outbreaks in the Midwest, which was seen during the winter months in 2013 (Figure 6), was deepened by the Pacific ridge.

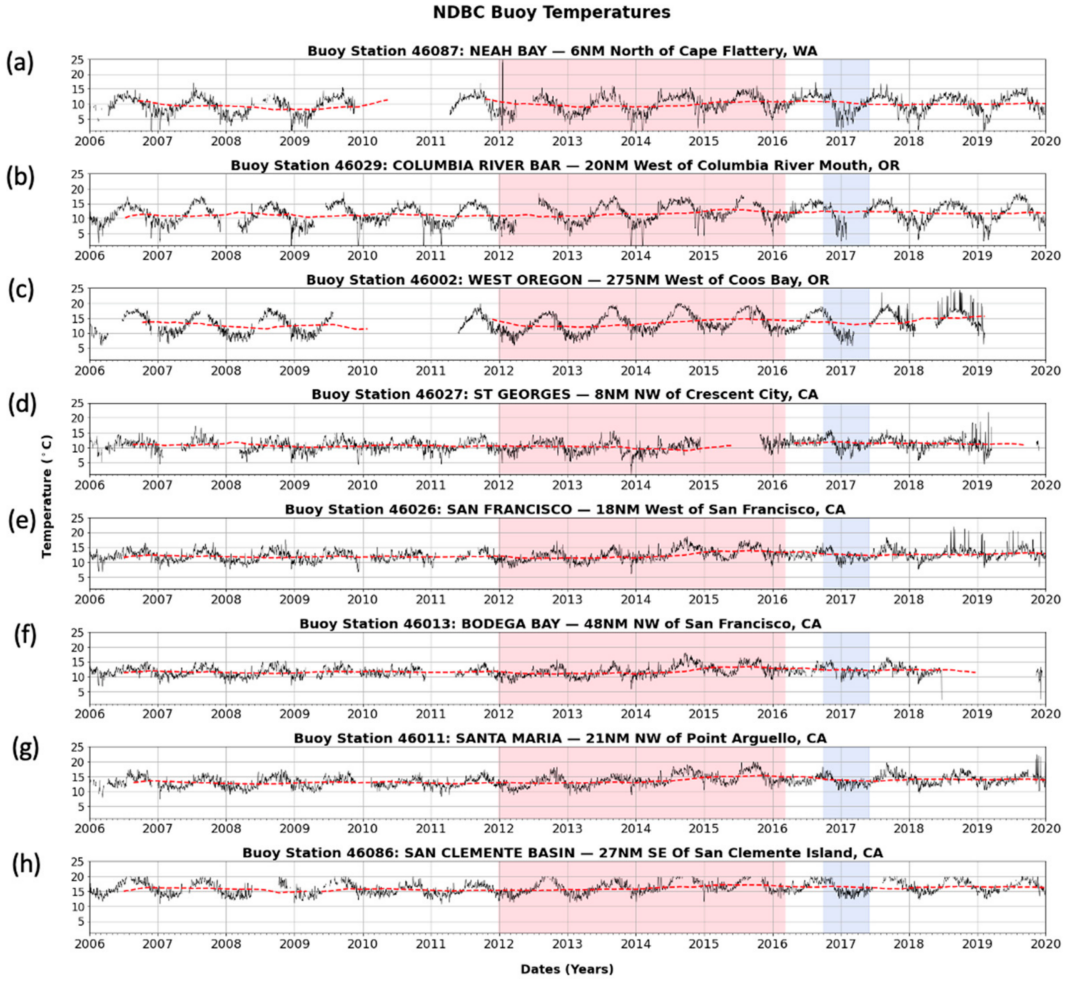

Figure 5. NDBC Buoy temperatures data for eight locations within the focus area: (**a**) West Oregon—275NM West of Coos Bay, OR, USA, (**b**) Santa Maria—21NM NW of Point Arguello, CA, USA, (**c**) Bodega Bay—48NM NW of San Francisco, CA, USA, (**d**) San Francisco—18NM West of San Francisco, (**e**) St. Georges—8NM NW of Crescent City, CA, USA, (**f**) Columbia River Bar—20NM west of Columbia River Mouth, (**g**) San Clemente Basin—27NM SE of San Clemente Island, CA, USA, and (**h**) Neah Bay—6 NM North of Cape Flattery, WA, USA). The area shaded in red highlights the third worst drought in California, while the extreme rain season is shaded in blue.

In the autumn of 2013, weak negative height and thickness anomalies were found in California due to the remnants of a late summer monsoon; however, drought conditions returned to the desert southwest in DJF and persisted into the spring months. In 2015, geopotential height anomalies dropped back to 2006–2011 climatological average values. An eastern push of the 500 hPa trough was observed in the autumn of 2016 west of Washington, with anomalies bottoming out at −6.66 decameter (dm) in region 1, −3.98 dm in region 2, and −1.97 dm in region 3, and remaining near normal (−0.09 dm) in region 4. (Table 1a). Thickness anomalies in SON 2016 saw a −2.78 dm anomaly in region 1, −1.75 dm in region 2, −1.10 dm in region 3, and −0.10 dm in region 4 (Table 1c). This eastward track of the upper-level longwave trough was crucial in the development of an above average rain season in 2016. In DJF 2016, low geopotential height and thickness anomalies persisted along the northwestern United States with −3.78 dm in region 1, −5.67 dm in region 2, −2.03 dm in region 3, and −2.00 dm in region 4 (Table 1b). In terms

of thickness during DJF 2016, region 1 observed a −4.07 dm anomaly, while this was −4.09 dm in region 2, −0.59 dm in region 3, and −0.69 dm in region 4 (Table 1d). In 2017, SON observed near normal height anomalies (Table 1a); however, there was the return of a resilient ridge with positive anomalies in DJF around positive 5 to 7 dm. The resilience of the winter ridge in 2017–2018 inevitably pushed the storm track further into Canada, hence dramatically decreasing the western United States' precipitation. Subsequently, in 2018, near-zero anomalies were found in autumn; however, a negative 2–4 dm anomaly developed. The wintertime trough helped drop the storm track further south to the California-Oregon border in late winter and spring, which yielded multiple atmospheric river events and an above average rain season in 2018–2019.

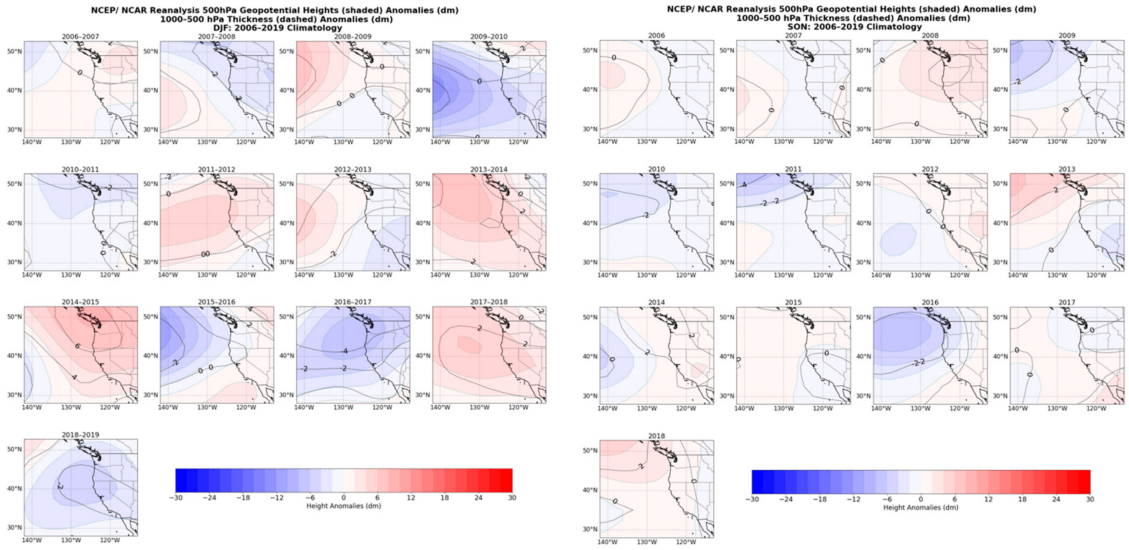

(**a**) (**b**)

Figure 6. NCEP Reanalysis of 500 hPa geopotential heights and 1000–500 hPa anomalies from 2006 through 2019 for (**a**) September, October, November (SON), and (**b**) December, January, February (DJF).

Table 1. 500 hPa geopotential height anomalies (decameter; dm) for (**a**) SON and (**b**) DJF, and 1000–500 hPa thickness anomalies for (**c**) SON and (**d**) DJF from 2006 through 2019. Color range in table reflects each region seasonal mean as seen in Figure 6.

(a)				
SON: 500 mb Geopotential Height Mean Anomalies				
Year	**Region 1**	**Region 2**	**Region 3**	**Region 4**
2006	1.18	−0.35	0.92	−0.11
2007	0.23	−0.50	1.21	−0.04
2008	1.46	3.37	1.40	2.00
2009	−3.97	−1.51	−0.02	0.34
2010	−3.29	−1.87	−0.35	−0.20
2011	−2.70	−1.34	0.36	0.12
2012	−0.91	0.70	−1.59	0.10
2013	3.20	1.26	0.57	−0.44
2014	−1.41	1.15	−1.29	1.40
2015	0.93	0.57	0.88	0.19
2016	−6.66	−3.98	−1.97	−0.09
2017	0.12	−0.28	0.27	1.18
2018	2.43	1.84	0.70	1.09

Table 1. *Cont.*

(b)				
DJF: 500 mb Geopotential Height Mean Anomalies				
Year	**Region 1**	**Region 2**	**Region 3**	**Region 4**
2006–2007	1.04	2.04	2.65	1.53
2007–2008	0.95	−2.10	3.32	0.57
2008–2009	5.71	1.68	2.60	0.53
2009–2010	−5.93	−2.36	−5.95	−3.65
2010–2011	−0.50	−1.41	0.71	0.05
2011–2012	5.25	4.63	5.39	3.52
2012–2013	4.12	0.88	3.59	0.01
2013–2014	8.04	5.55	5.19	4.94
2014–2015	5.22	7.55	2.23	4.64
2015–2016	−5.40	−1.13	−0.49	1.84
2016–2017	−3.78	−5.67	−2.03	−2.00
2017–2018	7.05	5.31	5.37	5.08
2018–2019	−0.71	−3.30	−1.40	−2.17
(c)				
SON: 1000–500 hPa Thickness Mean Anomalies				
Year	**Region 1**	**Region 2**	**Region 3**	**Region 4**
2006	0.16	−0.23	0.42	−0.26
2007	−0.83	−1.27	0.51	−0.33
2008	1.00	2.07	1.08	1.53
2009	−1.86	−0.77	−0.04	0.46
2010	−2.07	−1.45	−0.75	−0.64
2011	−1.99	−1.08	−0.01	−0.11
2012	−0.54	0.91	−1.02	−0.12
2013	1.78	0.81	0.71	−0.15
2014	1.78	2.68	1.34	2.40
2015	0.46	0.68	0.86	0.54
2016	−2.78	−1.75	−1.10	−0.10
2017	0.22	0.46	0.71	1.60
2018	1.86	1.34	0.71	1.30
(d)				
DJF: 1000–500 hPa Thickness Mean Anomalies				
Year	**Region 1**	**Region 2**	**Region 3**	**Region 4**
2006–2007	−0.16	0.38	−0.14	−0.53
2007–2008	−0.47	−1.98	0.99	−0.24
2008–2009	1.77	0.20	0.65	0.15
2009–2010	0.73	1.02	−0.49	−0.55
2010–2011	−1.17	−1.25	0.06	0.32
2011–2012	1.40	1.53	1.61	1.32
2012–2013	0.09	−1.10	−0.70	−1.80
2013–2014	4.09	2.63	3.60	4.07
2014–2015	5.50	6.43	3.95	5.00
2015–2016	−0.81	0.60	0.54	1.49
2016–2017	−4.07	−4.09	−0.59	−0.69
2017–2018	2.72	2.17	2.76	3.39
2018–2019	−0.64	−1.79	−0.66	−1.11

3.2.2. Sea Level Heights

The second variable analyzed within the target area was NASA MEaSUREs [21] sea level heights (Figure 7a,b and Table 2). In this section, the target area was broken into four sub-regions to quantify how the sea level heights changed and to explain which location may be critical in enhancing western US precipitation.

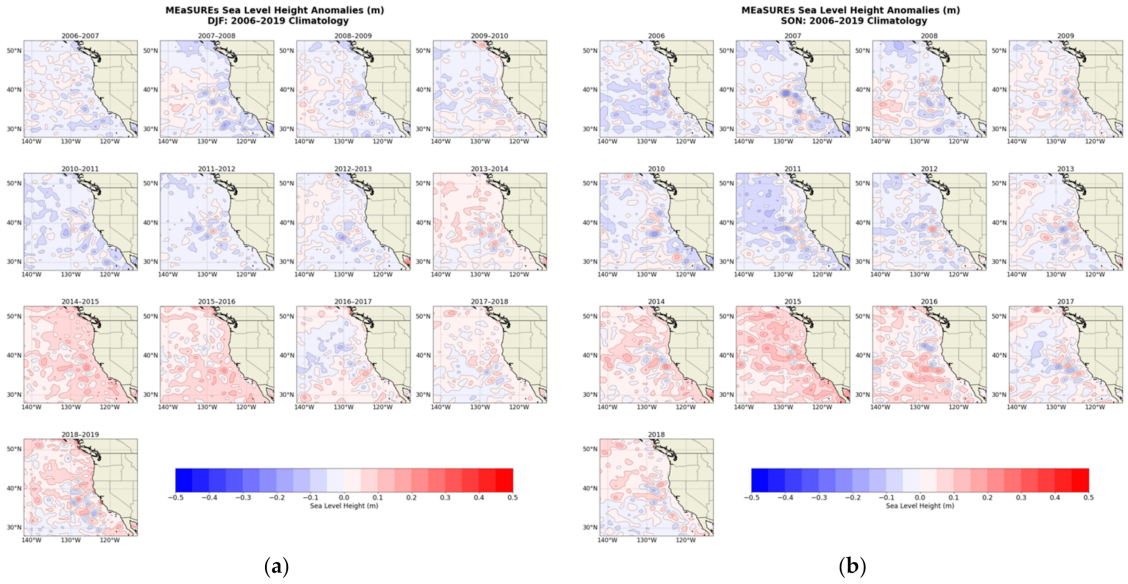

(**a**) (**b**)

Figure 7. Making Earth System Data Records for Use in Research Environments (MEaSUREs) sea level height anomalies from 2006 through 2019, valid for (**a**) SON and (**b**) DJF.

In terms of sea level heights during the SON months for the targeted timespan (Figure 7a), the northeastern Pacific observed positive sea level height anomalies in all four domains, except for region 1 in 2011, which had a value of −0.015 (Table 2a). The DJF months shows a tale of two different outcomes. During the 2006–2012 timespan, DJF sea level heights had negative anomalies in almost all years and regions except for region 3 from 2007–2010 (Figure 7b). The minimum DJF sea level height occurred in 2010 for all regions, with values at −0.041 m in region 1, −0.037 m in region 2, −0.022 m in region 3, and −0.036 m in region 4 (Table 2b). To further analyze the sub-regional changes in sea level heights per year, the average seasonal percentage change was calculated (Table 3).

As shown in Table 3, a positive percentage change rate between 2012 and 2015 coincides with the beginning of the 3-year long west coast drought. In 2013, sea level heights observed the biggest percentage change of 8650%, and the ocean surface warmed. This result is consistent with the regional average buoy and COSMIC temperatures rise during the west coast drought. In the period 2014–2015, both SON (0.111 m) and DJF (0.061 m) observed the highest sea level heights, with an annual average of 0.086 m. In 2016, SON average sea level height anomalies measured 0.072 m; however, in contrast to high heights in 2015, 2016 DJF decreased substantially to 0.001 m. The tremendous decrease of sea level heights in DJF was directly related to an extreme atmospheric river rain season due to an increase in the total amount of storms. Heights continued to fall by another 40% through the end of 2017. After a dry and warm 2018, another bump of 78% in sea level heights can be seen, which positively influenced another above average precipitation year in 2018–2019.

To verify the patterns and trends within the sea level height data, each of the four subdomains were compared using an annual time series (Figure 8). A noteworthy point is that the sea level heights annual trend line shows a similar possible oscillation to the COSMIC mixing ratio (Figure 3). This observation was crucial for showing a potential link between sea level heights and COSMIC mixing ratio due to the thermal expansion/compression of the ocean (e.g., Widlansky et al. 2020) [30]. In order to explain the variations of SLH

anomalies, a deeper look into the Oceanic Niño Index (Climate Prediction Center 2020) [24] was required. The ENSO categorial strength explains that, during the western United States drought, ENSO fluctuated between a moderate La Niña in 2011–2012 and a weak El Niño in 2014–2015. During the wet season of 2016–2017, a weak La Niña returned for the west coast. Further analysis of the relationships between variables can be seen in the linear regression section later (Section 3.2.4).

Table 2. Quantitative analysis of sea level heights anomalies from 2006 through 2019 for (**a**) SON and (**b**) DJF. Color range in table reflects each region seasonal mean as seen in Figure 7.

(a)				
SON: Sea Level Height Mean Anomalies				
Year	**Region 1**	**Region 2**	**Region 3**	**Region 4**
2006	0.035	0.011	0.005	−0.002
2007	0.035	0.017	0.047	0.010
2008	0.039	0.021	0.059	0.016
2009	0.059	0.034	0.054	0.027
2010	0.029	0.021	0.030	0.016
2011	−0.015	0.017	0.016	0.002
2012	0.030	0.011	0.023	0.016
2013	0.058	0.028	0.044	0.021
2014	0.096	0.078	0.077	0.070
2015	0.134	0.106	0.097	0.105
2016	0.078	0.041	0.087	0.083
2017	0.041	0.047	0.042	0.036
2018	0.090	0.062	0.052	0.040
(b)				
DJF: Sea Level Height Mean Anomalies				
Year	**Region 1**	**Region 2**	**Region 3**	**Region 4**
2006–2007	−0.008	−0.027	−0.013	−0.020
2007–2008	−0.008	−0.038	0.013	−0.033
2008–2009	−0.004	−0.031	0.003	−0.027
2009–2010	−0.011	−0.006	0.010	0.004
2010–2011	−0.041	−0.037	−0.022	−0.024
2011–2012	−0.032	−0.024	−0.022	−0.036
2012–2013	−0.021	−0.030	−0.012	−0.015
2013–2014	0.038	−0.006	0.009	−0.017
2014–2015	0.043	0.066	0.044	0.064
2015–2016	0.046	0.046	0.068	0.084
2016–2017	−0.024	−0.011	0.019	0.020
2017–2018	−0.000	0.007	0.003	0.009
2018–2019	0.026	0.026	0.021	0.013

Table 3. MEaSUREs annual percentage change of sea level heights in the target area.

SLH (m)				
Year	**SON**	**DJF**	**Mean**	**% Change (m/year)**
2006	0.012	−0.017	−0.002	-
2007	0.027	−0.017	0.005	326.3
2008	0.034	−0.015	0.010	76.7
2009	0.044	−0.001	0.021	125.0
2010	0.024	−0.031	−0.004	−116.4
2011	0.005	−0.021	−0.008	−125.0
2012	0.020	−0.020	0.000	103.2
2013	0.038	0.006	0.022	8650.0
2014	0.080	0.054	0.067	207.4
2015	0.111	0.061	0.086	27.5
2016	0.072	0.001	0.037	−57.3
2017	0.042	0.005	0.023	−37.8
2018	0.061	0.022	0.041	78.3

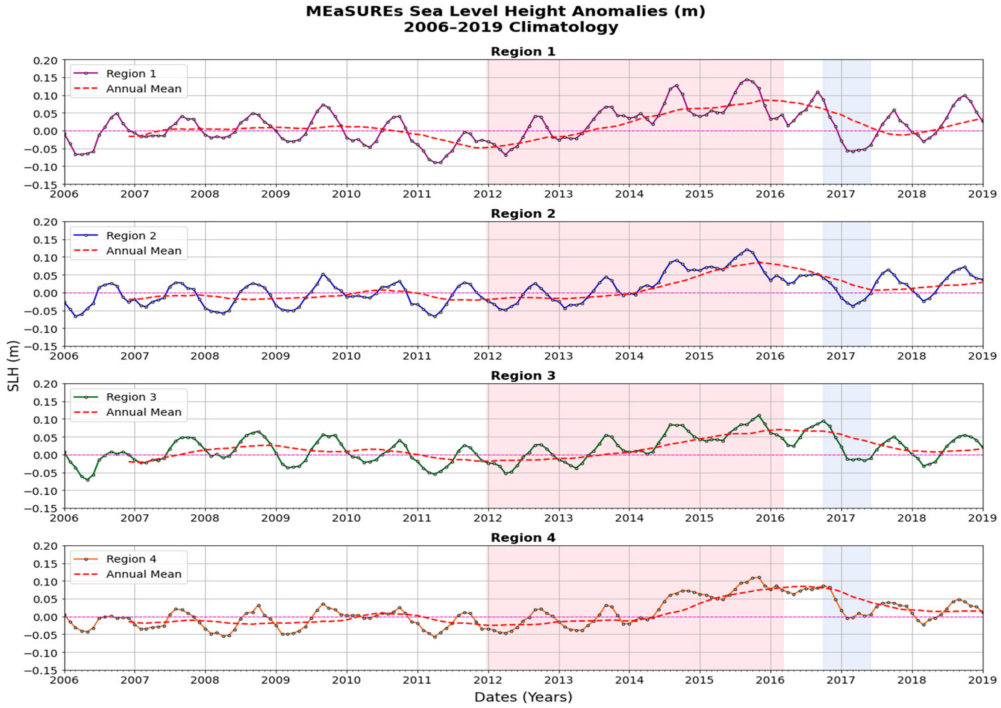

Figure 8. Time series of sea level heights from 2006 through 2019. The shaded area in red highlights the third worst drought, while the extreme rain season is shaded in blue.

3.2.3. Sea Surface Temperatures

The third and final variable, analyzed in Figure 9a,b, is sea surface temperatures (SSTs) from the NOAA 1/4° daily Optimum Interpolation (OI) Sea Surface Temperature (SST) Version 2 data. Sea surface temperatures between 2006 and 2012 observed negative anomalies between 0 and −1 °C. In the period 2013–2014, the large-scale pattern in both autumn and winter shifted from negative anomalies and became positive (Figure 9). The eastern Pacific detected a push of warmer water poleward; however, it persisted away from the coast in regions 1 and 3. In 2014, SST anomalies for both autumn and winter warmed between positive 1–2 °C and persisted through the DJF of 2016 (Table 4. El Niño typically leads to above average precipitation in California; however, the west coast observed near normal precipitation amounts in 2014 and 2015. According to the Oceanic Niño Index (Table 5) [31], 2014–2015 observed a weak El Niño (SST anomalies 0.5 to 0.9) and a strong

El Niño (SST anomalies 1.5 to 1.9) in 2015–2016. Patricola et al. (2019) and Quan et al., (2018) [31,32] suggested that one possible reason for this was due to the internal atmospheric variability. The peak of SST occurred in 2015, which was verified with the highest annual average amplitude of 2.5 in the ENSO Oscillation [24]. In 2016, a return of cooler SSTs (-1 to -1.5 °C) in regions 1 and 2 and negative (-0.7 to -0.3) ENSO amplitudes were found. Furthermore, the Oceanic Niño Index (Table 5) [24], 2016–2017 saw a weak La Niña (SST anomalies -0.5 to -0.9), and a strong La Niña (SST anomalies -1.5 to -1.9) was observed in 2017–2018. The drop off of SST prior to the extreme 2016–2017 rain season can be explained by a more atmospheric river events and the occurrence of storms, which consequently led to more latent heat release into the atmosphere from the ocean surface. Therefore, the extra heat from the ocean surface that was transferred into the atmosphere would directly lead to an increase of moisture into the atmosphere, which is consistent with the COSMIC vertical profiles shown earlier (Figure 2). In 2017, the eastern Pacific observed another push of warm positive anomalies poleward; however, the mid-level ridge (Figure 6) did allow the transport of moisture to the west. On the other hand, in 2018, similar warm SST anomalies were found within the target region, but the mid-level trough tapped into the subtropical moisture, consequently producing another active rain season in 2018–2019.

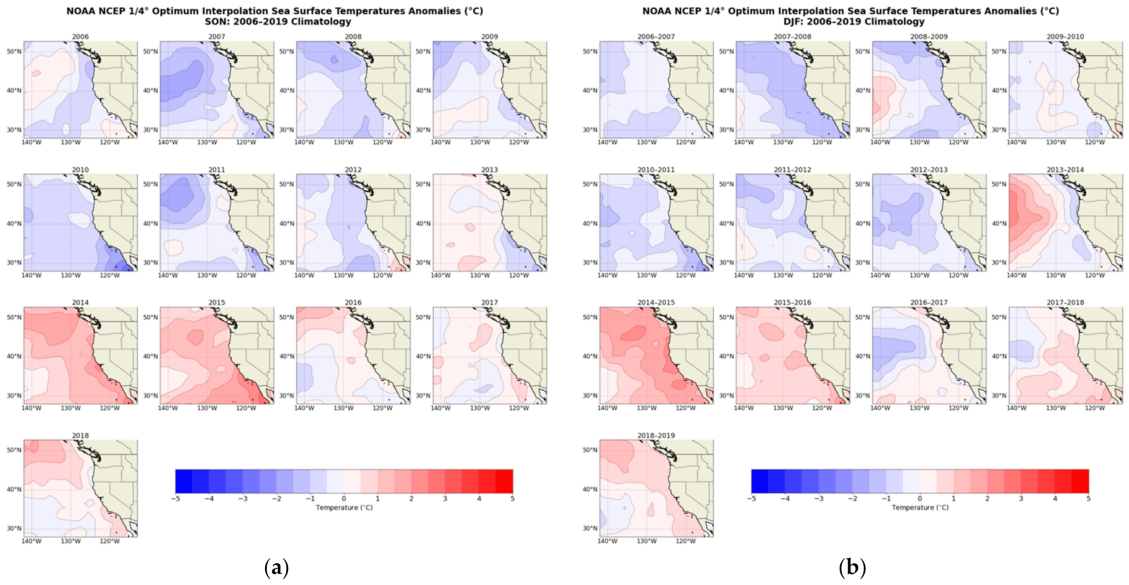

Figure 9. NOAA Optimum Interpolation (OI) sea surface temperature anomalies from 2006–2019 valid for (**a**) SON and (**b**) DJF.

3.2.4. Statistics—Linear Regression

Linear regression was performed to identify the statistical significance of each variable that may have influenced the western United States precipitation. Analysis in this section compares the annual average of the four subdomains for sea surface temperature v. sea level heights (Figure 10a) and the NASA MEaSUREs sea level heights v. COSMIC mixing ratio (Figure 10b). Sea surface temperatures and sea level heights have a strong correlation coefficient of $R^2 = 0.50$. The direct influence of SST and SLH are related to expansion and/or contraction as ocean temperature increases and/or decreases. Sea level height and mixing ratio had the highest correlation coefficient of $R^2 = 0.65$. This finding suggests that, as sea level heights increase, COSMIC's mixing ratio increases, verifying that there is a direct impact to the overall moisture field forced by more latent heat released into the atmosphere.

Table 4. Sea surface temperature anomalies (°C) from 2006–2019 for (**a**) SON and (**b**) DJF. Color range in table reflects each region seasonal mean as seen in Figure 9.

(**a**)

SON: Sea Surface Temperature Mean Anomalies				
Year	**Region 1**	**Region 2**	**Region 3**	**Region 4**
2006	0.22	−0.50	−0.28	−0.39
2007	−1.41	−0.67	−0.75	−0.38
2008	−0.73	−0.63	−0.30	−0.75
2009	−0.56	−0.30	−0.00	−0.34
2010	−0.69	−0.45	−0.66	−0.84
2011	−1.25	−0.22	−0.21	−0.28
2012	−0.42	−0.48	−0.21	−0.50
2013	0.11	−0.01	0.44	−0.20
2014	1.55	1.34	0.73	1.52
2015	1.32	1.21	0.79	1.56
2016	0.35	0.49	−0.18	0.23
2017	0.26	0.32	0.15	0.13
2018	0.85	0.33	−0.02	0.25

(**b**)

DJF: Sea Surface Temperature Mean Anomalies				
Year	**Region 1**	**Region 2**	**Region 3**	**Region 4**
2006–2007	−0.45	−0.29	−0.30	−0.48
2007–2008	−1.12	−1.03	−0.35	−1.10
2008–2009	−0.38	−0.75	0.17	−0.59
2009–2010	−0.13	−0.04	0.00	−0.09
2010–2011	−0.75	−0.50	−0.50	−0.50
2011–2012	−0.79	−0.59	−0.17	−0.31
2012–2013	−0.96	−0.38	−0.48	−0.42
2013–2014	1.14	−0.31	0.65	−0.27
2014–2015	1.72	1.62	1.05	1.85
2015–2016	0.88	0.91	0.76	0.90
2016–2017	−0.79	0.06	0.02	0.13
2017–2018	−0.12	0.50	0.49	0.58
2018–2019	0.79	0.69	0.07	0.55

3.2.5. Atmospheric Rivers and Precipitation

The final set of analysis incorporates the Hecht and Ralph (2020) [33–35] classification of the total number of AR storms sorted by the location where they made landfall since 2016 and comparing it to the reanalysis data (Table 6). As explained using the geopotential height and thickness fields, in 2016 the eastward push of the 500 hPa trough to the Pacific Northwest (Figure 6), directly affected the total number of AR storms and their landfalling location. Hecht and Ralph (2020) conclude that 2016 had a total of 50 atmospheric rivers occurring, with 5 landfalling in southern California (S. CA), 4 in central California (C. CA), 16 in northern California (N. CA), 15 in Oregon (OR), and 10 in Washington (WA). Following

the extreme rain year of 2016–2017, the total number of ARs in 2017–2018 dropped to 31, with most AR events landfalling in Washington, Oregon, and the top of California as a persistent ridge settled along the western United States (Figure 6). In addition to a persistent ridge, the target area observed a decrease in both sea surface temperatures (Figure 9) and sea level heights (Figure 7). In 2018–2019, another eastward push of the 500 hPa geopotential heights and thicker and warmer SSTs allowed for another above average rain season, with a total of 41 AR events occurring. The 2018–2019 rain season saw similar results to the extreme AR year of 2016–2017 in terms of predominant landfalling locations in northern California and Oregon. This can be explained by the dip southward of the mid-level trough, which allowed ARs to track further south (Figure 6).

Table 5. ENSO amplitudes from 2006 through 2018 to show the comparison with seasonal sea surface temperatures.

ENSO Amplitudes			
Year	**SON**	**DJF**	**Mean**
2006	0.7	0.7	0.7
2007	−1.4	−1.6	−1.5
2008	−0.4	−0.8	−0.6
2009	1.0	1.5	1.3
2010	−1.7	−1.4	−1.6
2011	−1.1	−0.8	−1.0
2012	0.2	−0.4	−0.1
2013	−0.2	−0.4	−0.3
2014	0.4	0.6	0.5
2015	2.4	2.5	2.5
2016	−0.7	−0.3	−0.5
2017	−0.7	−0.9	−0.8
2018	0.7	0.8	0.8

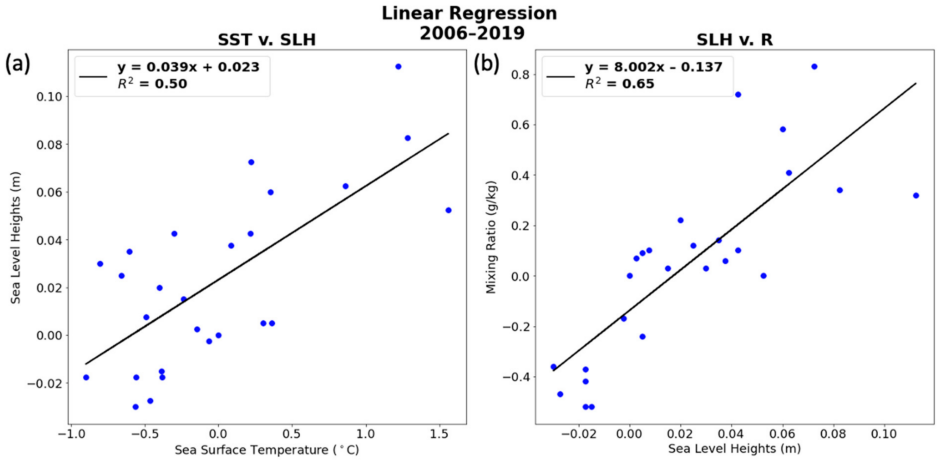

Figure 10. Linear regression of (**a**) sea surface temperature v. sea level heights and (**b**) sea level heights v. COSMIC mixing ratio.

To further verify precipitation and AR events, a comparison between the total number of ARs with the total annual precipitation for five northern and central California locations from 1 October through 31 March was analyzed (NCEI 2020) [36]. In Figure 11, each of the five locations observed substantially wide ranges of total annual precipitation due to a variety of orographic effects. San Jose, which is located in a rain shadow of the Santa Cruz Mountains, received about 10.7 inches on average over the 13-year period (Figure 11a). Next, Santa Cruz, a beach city southwest of the Santa Cruz Mountains that observes some orographic enhancement, received approximately 24.1 inches annually (Figure 11b).

Similar to Santa Cruz's orographic effects, Monterey, a beach city along the California central coast, collected around 13.9 inches (Figure 11c). San Francisco International Airport (KSFO), located along the San Francisco Peninsula, obtained roughly 15.4 inches per year (Figure 11d). Finally, Big Sur, a mountainous part of the California central coast, acquired about 33.2 inches of precipitation every year (Figure 11e). A key finding revealed from annual precipitation data was that, when the annual running mean was calculated, a similar wave-like pattern could be observed, which is similar to the COSMIC mixing ratio heatmap (Figure 3) and the northeastern Pacific sea level heights (Figure 8).

Table 6. Number of landfalling Atmospheric Rivers (ARs) along the western US, broken into five separate locations Southern California (S. CA), Central California (C. CA), Northern California (N. CA), Oregon (OR), and Washington (WA).

Total Number of Landfalling AR Storms						
WY	**S. CA**	**C. CA**	**N. CA**	**OR**	**WA**	**Total**
2016–2017	5	4	16	15	10	50
2017–2018	1	2	10	10	8	31
2018–2019	3	4	13	14	6	41
2019–2020	4	3	5	10	18	40

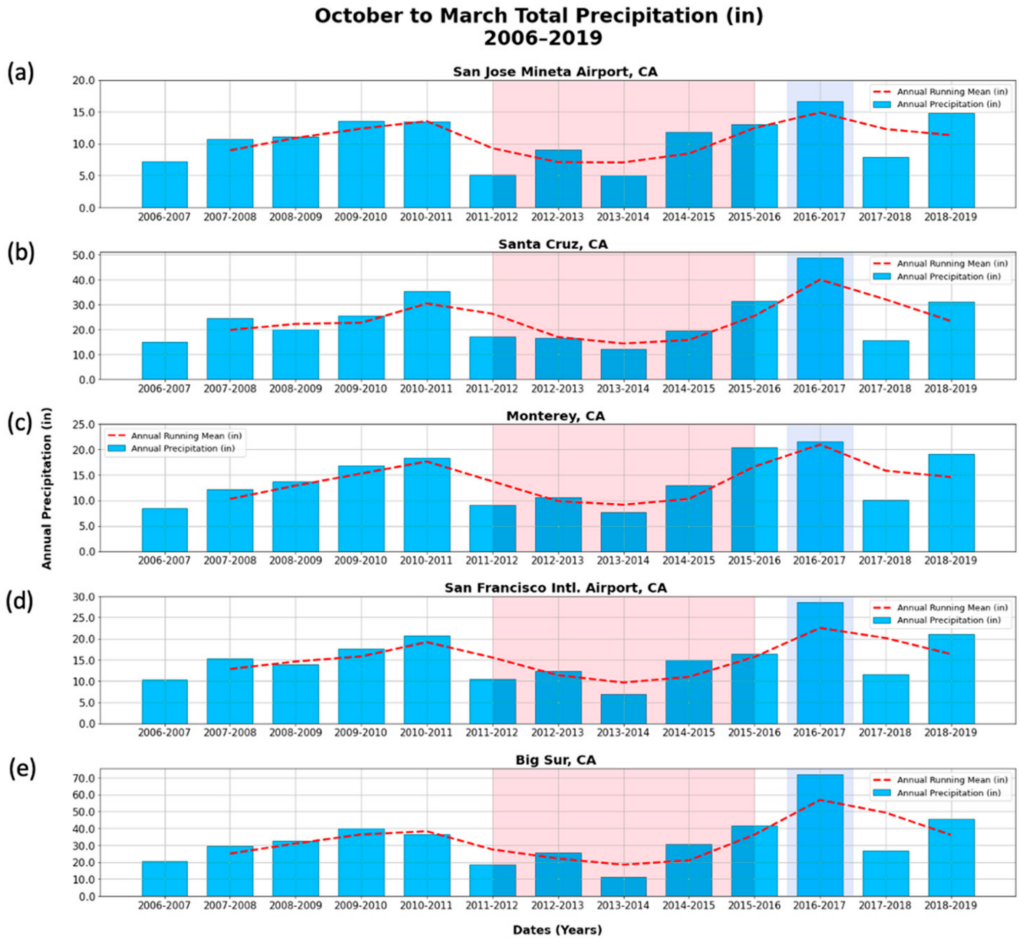

Figure 11. Annual precipitation for (**a**) San Jose Mineta Airport, (**b**) Santa Cruz, CA, USA, (**c**) Monterey, CA, USA, (**d**) San Francisco International Airport, and (**e**) Big Sur, CA, USA. Areas shaded in red highlight the third worst drought, while the extreme rain season is shaded in blue.

4. Discussion and Summary

Annual precipitation, regional reanalysis of geopotential height, 1000–500 hPa thickness, sea surface height anomalies, sea surface temperature, and COSMIC moisture and temperature profiles were evaluated in this study from 2006 to 2019. The study included the third worst drought, from 2012–2014, and compared and contrasted the dynamical changes to the extreme AR wet seasons of 2016–2017 in California. This study was designed to evaluate the COSMIC data and how it can be used to improve our current understanding of AR occurrence along the west coast. COSMIC has provided a quantification of high-resolution vertical profiles in terms of pressure, vapor pressure, and temperature throughout the mid-latitudes and tropics. This quantification assists and builds on the scientific knowledge concerning how likely it is that the regional changing climate has directly affected the moisture and temperature fields. Understanding the prior thirteen years (2006–2019) of data can provide a public insight into what can be expected in terms of precipitation along the western United States.

The COSMIC mixing ratio time series showed a slight decreasing trend ~−0.19 g/kg (~−0.047 g/kg/year) from July 2006 through early 2013 (Figure 2). During the period 2006 to 2013, COSMIC temperatures showed a similar decreasing trend of ~−2.10 °C (~−0.52 °C/year). In late 2015 to 2016, the mixing ratio showed the steepest climb of ~0.32 g/kg (~0.162 g/kg/year). Buoy temperatures from NDBC in the Northeastern Pacific during the period 2014–2015 showed temperatures peaking between 17–20 °C; however, the COSMIC temperature vertical profiles observed the warmest temperatures in 2016, which matched the strongest El Nino and NOAA warmest year on record. In 2016 and 2017, the mixing ratio peaked and stayed constant at ~2.8 g/kg. Results suggested that increasing global temperatures tend to lead to an increase of heat fluxes into the atmosphere, consequently increasing moisture within the target area. Therefore, moisture from an increase of latent heat release by warmer SSTs, as suggested by Chen and Leung (2020) and Dai et al. (1998) [8,9] and the total frequency and strength of AR could potentially increase, as was seen on the west coast in 2016–2017. In 2018, mixing ratios dipped by ~0.2 g/kg and stayed constant till the end of the studied period in March of 2019. Another interesting finding using the COSMIC mixing ratio heatmaps from October to March was that they revealed a wave-like pattern. In order to show how increasing moisture changes AR frequency and strength, the total number of ARs and the total annual precipitation for five California cities were compared to the COSMIC mixing ratio data (Figure 11). It can be explained by the winter trough during the active wet seasons. In above average rain seasons, the trough transports moisture into the atmosphere from warmer SSTs and less moisture and convection from cooler SSTs during droughts. A noteworthy feature from the annual precipitation analysis showed another similar wave pattern to the COSMIC mixing ratios (Figure 3).

The analysis of climatological regional scale factors found that the most efficient and useful variable relating to AR frequency was sea level height anomalies. Furthermore, sea level height anomalies had the highest correlation coefficient of $R^2 = 0.65$ with the COSMIC mixing ratio. Consistent with meteorological theory, sea level heights rose due to the enhanced warming during the drought, consequently increasing evaporation and providing more vapor to the atmosphere. The link between sea surface temperature and mixing ratio has been asserted for years. This study found that 50% of the variation of sea surface temperature ($R^2 = 0.50$) was attributed to sea level heights. Because sea surface temperatures lag behind the seasonal air temperature due to the high specific heat capacity of water, it appears that having a warmer summer and autumn can allow more moisture to be lofted into the atmosphere for the following rain season. Sea surface temperature can directly impact the location of mid-level troughs and ridges, as observed within the geopotential height and thickness fields. In terms of the drought, cooler sea surface temperatures prevailed, which allowed a persistent 500 hPa ridge to advect over the western United States and lead to a below average rain season. On the other hand, during the strong AR year in 2016–2017, the west observed warmer sea surface temperatures

that pushed the mid-level trough eastward toward the Pacific Northwest, allowing for the surface low to propagate over the west coast, leading to an above-average rain season.

The findings from this study provide new information to the scientific community about which atmospheric factors are beneficial to droughts and ARs. In this experiment, we acknowledge that 13 years of COSMIC satellite data may not be sufficient to analyze the climate variability of droughts and ARs. In order to extend the studied timespan, future experiments should include the new COSMIC-2 satellite, which was launched in June 2019. Potentially in the future, this research should help forecasters and water managers develop seasonal forecasts. Therefore, continued work moving the domain to another location to verify the northeastern Pacific sinusoidal wave-pattern is recommended. A future research study with COSMIC-2 and monthly climatology of SST and SLH data promises future developments for seasonal forecasting. The warranted study could include the relationship between several climate indices (i.e., El Niño Southern Oscillation (ENSO), Arctic Oscillation (AO), and Pacific Decadal Oscillation (PDO)) and COSMIC mixing ratios. The potential linkage with climatological indices could help improve the forecast of enhanced AR years and droughts nearly three months ahead of a given season. In summary, we recommend continued research using COSMIC-2 data within the Weather Research and Forecasting (WRF) model to provide a lasting benefit and better understanding of AR forecasting.

Author Contributions: Conceptualization, P.R.Z. and S.C.; methodology, S.C.; software, P.R.Z.; validation, P.R.Z. and S.C.; formal analysis, P.R.Z. and S.C.; investigation, P.R.Z. and S.C.; resources, P.R.Z.; data curation, P.R.Z.; writing—original draft preparation, P.R.Z. and S.C.; writing—review and editing, P.R.Z. and S.C.; visualization, P.R.Z.; supervision, S.C.; project administration, S.C.; funding acquisition, S.C. All authors have read and agreed to the published version of the manuscript.

Funding: This study was supported by the NASA MUREP grant (NNX15AQ02A), and the Center for Applied Atmospheric Research and Education (CAARE) at San Jose State University.

Data Availability Statement: The data presented in this study are available on request from the corresponding author.

Acknowledgments: The authors acknowledge all of the suppliers of the datasets employed in this study. We also appreciate discussions and valuable suggestions made by NCAR scientists Ying-Hwa Kuo and Zhiquan Liu. Finally, we would like to acknowledge our reviewers on making insightful comments and suggestions to improve the manuscript.

Conflicts of Interest: The authors declare no conflict of interest.

References

1. Neiman, P.J.; Ralph, F.M.; Wick, G.A.; Kuo, Y.-H.; Wee, T.-K.; Ma, Z.; Taylor, G.H.; Dettinger, M.D. Diagnosis of an intense atmospheric river impacting the Pacific Northwest: Storm summary and off-shore vertical structure observed with COSMIC satellite retrievals. *Mon. Weather Rev.* **2008**, *136*, 4398–4420. [CrossRef]
2. Rutz, J.J.; Steenburgh, W.J.; Ralph, F.M. Climatological characteristics of atmospheric rivers and their inland penetration over the western United States. *Mon. Weather Rev.* **2014**, *142*, 905–921. [CrossRef]
3. Dettinger, M.D. Atmospheric rivers as drought busters on the US West coast. *J. Hydrometeorol.* **2013**, *14*, 1721–1732. [CrossRef]
4. Dettinger, M.D. Climate change, atmospheric rivers, and floods in California—A multimodel analysis of storm frequency and magnitude changes. *JAWRA* **2011**, *47*, 514–523. [CrossRef]
5. Anthes, R.; Rocken, C.; Kuo, Y.-H. Applications of COSMIC to meteorology and climate. *Terr. Atmos. Ocean. Sci.* **2001**, *11*. [CrossRef]
6. Wang, K. Climate change detection with the global GPS information system. *Environ. Sci. DEStech Trans. Eng. Technol. Res.* **2017**. [CrossRef]
7. Trenberth, K.E.; Guillemot, C.J. Physical processes involved in the 1988 drought and 1993 floods in North America. *J. Clim.* **1996**, *9*, 1288–1298. [CrossRef]
8. Chen, X.; Leung, L. Response of landfalling atmospheric rivers on the U.S. West Coast to local sea surface temperature perturbations. *Geophys. Res. Lett.* **2020**, *47*. [CrossRef]
9. Dai, A.; Trenberth, K.E.; Karl, T. Global variations in droughts and wet spells: 1900–1995. *Geophys. Res. Lett.* **1998**, *25*, 3367–3370. [CrossRef]

10. Koutavas, A.; DeMenocal, P.B.; Olive, G.C.; Lynch-Stieglitz, J. Mid-Holocene El Niño-Southern Oscillation (ENSO) attenuation revealed by individual foraminifera in eastern tropical Pacific sediments. *Geology* **2006**, *34*, 993–996. [CrossRef]
11. Stott, L.; Cannariato, K.; Thunell, R.; Haug, G.H.; Koutavas, A.; Lund, S. Decline of surface temperature and salinity in the western tropical Pacific Ocean in the Holocene epoch. *Nature* **2004**, *431*, 56–59. [CrossRef] [PubMed]
12. Barron, J.A.; Heusser, L.; Herbert, T.; Lyle, M. High-resolution climatic evolution of coastal northern California during the past 16,000 years. *Paleoceanography* **2003**, *18*, 1–14. [CrossRef]
13. NOAA US Department of Commerce. What Is ENSO? Available online: https://www.weather.gov/mhx/ensowhat (accessed on 20 November 2020).
14. Penduff, T.; Llovel, W.; Close, S.; Garcia-Gomez, I.; Leroux, S. Trends of coastal sea level between 1993 and 2015: Imprints of atmospheric forcing and oceanic chaos. *Surv. Geophys.* **2019**. [CrossRef]
15. *Atmospheric Profiles from COSMIC Occultation Data*; Research Data Archive at the National Center for Atmospheric Research, Computational and Information Systems Laboratory: Boulder, CO, USA, 2013. Available online: https://rda.ucar.edu/datasets/ds723.0/ (accessed on 2 March 2020).
16. Ho, S.-P.; Anthes, R.A.; Ao, C.O.; Healy, S.; Horanyi, A.; Hunt, D.; Mannucci, A.J.; Pedatella, N.; Randel, W.; Simmons, A.; et al. The COSMIC/FORMOSAT-3 radio occultation mission after 12 years: Accomplishments, remaining challenges, and potential impacts of COSMIC-2. *Bull. Am. Meteorol. Soc.* **2019**. [CrossRef]
17. Constellation Observing System for Meteorology Ionosphere & Climate (COSMIC). Available online: https://www.nasa.gov/directorates/heo/scan/services/missions/earth/COSMIC.html (accessed on 10 April 2020).
18. UCAR Community Programs Global Navigation Satellite System Radio Occultation (GSNN_RO). Available online: https://www.cosmic.ucar.edu/what-we-do/gnss-radio-occultation/ (accessed on 16 March 2020).
19. COSMIC Data Analysis and Archive Center (CDAAC). Available online: https://cdaac-www.cosmic.ucar.edu/cdaac/products.html (accessed on 10 February 2020).
20. Kalnay, E.; Kanamitsu, M.; Kistler, R.; Collins, W.; Deaven, D.; Gandin, L.; Iredell, M.; Saha, S.; White, G.; Woollen, J.; et al. The NCEP/NCAR 40-year reanalysis project. *Bull. Am. Meteor. Soc.* **1996**, *77*, 437–470. [CrossRef]
21. *GHRSST Level 4 MUR Global Foundation Sea Surface Temperature Analysis (v4.1)*; NASA JPL: Pasadena, CA, USA, 2015. [CrossRef]
22. *Meteorological and Oceanographic Data Collected from the National Data Buoy Center Coastal-Marine Automated Network (C-MAN) and Moored (Weather) Buoys*; NOAA National Centers for Environmental Information: Boulder, CO, USA, 1971. Available online: https://ndbc.noaa.gov (accessed on 17 July 2020).
23. *JPL MEASURES Gridded Sea Surface Height Anomalies Version 1812*; NASA JPL: Pasadena, CA, USA, 2019. [CrossRef]
24. *Cold and Warm Episodes by Season*; National Weather Service: Silver Spring, MD, USA, 2020. Available online: https://origin.cpc.ncep.noaa.gov/products/analysis_monitoring/ensostuff/ONI_v5.php (accessed on 29 September 2020).
25. Null, J. El Niño and La Niña Years and Intensities. Available online: https://ggweather.com/enso/oni.htm (accessed on 29 December 2020).
26. Advanced Hydrologic Prediction Center. About the Precipitation Analysis Pages. Available online: https://water.weather.gov/precip/about.php. (accessed on 22 November 2020).
27. Phillips, B.; Leslie, J. International Report Confirms 2016 Was the Warmest Year on Record for the Globe. Available online: https://www.noaa.gov/news/international-report-confirms-2016-was-warmest-year-on-record-for-globe (accessed on 13 September 2020).
28. Swain, D.L. A tale of two California droughts: Lessons amidst record warmth and dryness in a region of complex physical and human geography. *Geophys. Res. Lett.* **2015**, *42*, 9999–10003. [CrossRef]
29. Wang, S.-Y.; Hipps, L.; Gillies, R.R.; Yoon, J.-H. Probable causes of the abnormal ridge accompanying the 2013–2014 California drought: ENSO precursor and anthropogenic warming footprint. *Geophys. Res. Lett.* **2014**, *41*, 3220–3226. [CrossRef]
30. Widlansky, M.J.; Long, X.; Schloesser, F. Increase in sea level variability with ocean warming associated with the nonlinear thermal expansion of seawater. *Commun. Earth Environ.* **2020**, *1*, 9. [CrossRef]
31. Patricola, C.M.; O'Brien, J.P.; Risser, M.D.; Rhoades, A.M.; O'Brien, T.A.; Ullrick, P.A.; Stone, D.A.; Collins, W.D. Maximizing ENSO as a source of western US hydroclimate predictability. *Clim. Dyn.* **2019**, *54*, 351–372. [CrossRef]
32. Quan, X.-W.; Hoerling, M.; Smith, L.; Perlwitz, J.; Zhang, T.; Hoell, A.; Wolter, K.; Eischeid, J. Extreme California rains during winter 2015/16: A change in El Niño teleconnection? *Bull. Am. Meteorol. Soc.* **2018**, *99*, S49–S53. [CrossRef]
33. Hecht, C.W.; Kawenuk, B.; Ralph, F.M. How Many Atmospheric Rivers Have Hit the U.S. West Coast During the Remarkably Wet Water Year 2017? Available online: https://cw3e.ucsd.edu/water-year-2019-december-atmospheric-rivers (accessed on 16 October 2020).
34. Hecht, C.W.; Ralph, F.M. Distribution of Landfalling Atmospheric Rivers over the U.S. West Coast during Water Year 2018: October through March Update. Available online: https://cw3e.ucsd.edu/distribution-of-landfalling-atmospheric-rivers-on-the-u-s-west-coast-during-water-year-2018/ (accessed on 16 October 2020).
35. Hecht, C.W.; Ralph, F.M. Distribution of Landfalling Atmospheric Rivers over the U.S. West Coast during Water Year 2020: October through March Update. Available online: https://cw3e.ucsd.edu/distribution-of-landfalling-atmospheric-rivers-over-the-u-s-west-coast-during-water-year-2020-october-through-march-update/ (accessed on 16 October 2020).
36. *NOAA Online Weather Data—Accumulated Precipitation*; National Weather Service: Silver Spring, MD, USA. Available online: https://w2.weather.gov/climate/xmacis.php?wfo=mtr (accessed on 19 August 2020).